Dynamics of the Reversible Inhibition during Methane Oxidation on Bimetallic Pd-Pt Catalysts Studied by Modulation-Excitation XAS and DRIFTS

Alexey Boubnov,*[a] Andreas Gremminger,[a] Maria Casapu,[a] Olaf Deutschmann,[a] and Jan-Dierk Grunwaldt*[a]

Water and NO reversibly inhibit catalytic methane oxidation to CO_2 over Pd/Al_2O_3 and $Pd-Pt/Al_2O_3$ at temperatures near 50% conversion. Modulation-excitation X-ray absorption spectroscopy (ME-XAS) was used to characterize the interaction of the inhibitors with the Pd and Pt components. Simulated X-ray absorption near-edge structure (XANES) spectra of Pd and Pt with various surface species were used to verify the findings of ME-XAS measurements. Diffuse-reflectance infrared Fourier-transform spectroscopy (DRIFTS) allowed to correlate methane oxidation with surface formate species. An interaction of water with active Pd sites and water coverage of the Al_2O_3 support caused a drastic drop in formate production, correlated with the observed inhibition. In a similar manner, nitrite groups formed from gas-phase NO inhibited the production of formates. At higher temperatures, the inhibition was reversed into a promoting effect by surface nitrates formed from NO that oxidized gas-phase methane. This approach is not only interesting for emission control but in general for catalysts where dynamic structural changes occur.

Introduction

Natural gas has recently gained interest as a logistic fuel due to its low price, its low CO_2 footprint and low sulfur emissions. In addition, it gains attention in so-call power-to-gas processes for energy storage purposes.[1] On the other hand, slip of unburned methane, which is the main constituent of natural gas, is strongly undesired due to its green-house effect, 20 times higher than that of CO_2. Methane is removed from the exhaust by oxidation over palladium-based catalysts and the process is effective at temperatures over 300°C.[2] With gas-motors that are more efficient the exhaust gas temperature will be lowered. However, at lower temperatures inhibition of the reaction both by water[3] and by nitrogen oxides[4] has been reported which,

at present, requires a sufficiently higher exhaust gas temperature in order to attain high conversions. Despite various studies have been conducted on the inhibition by these two reactants, the mechanisms of reaction and inhibition are still strongly discussed. A better understanding would give the possibility to improve the catalysts. This requires especially to analyze the dynamic structural changes occurring in such heterogeneous catalysts.[5]

Experimental and modelling studies have shown that water inhibits the catalytic combustion of methane especially below 450°C, shifting the light-off curve to higher temperatures.[6] This effect was observed for gas mixtures with both low and high content of water (0.1% to above 20%). The degree of inhibition increases with increasing water concentration. The inhibition has been debated to be caused by hydroxyl accumulation on the PdO phase, the support or at the noble metal-support interface, as shown by infrared spectroscopy.[3,7] However, the exact location of the hydroxyls and the interaction with the noble metal phase and the support are unknown, as it is very difficult to gain insight into the surface under realistic reaction conditions.

Nitrogen oxides are likewise known to inhibit methane oxidation below ca. 450°C and like in the case with water inhibition, the molecular interactions between the nitrogen oxide and the catalytic sites remain unresolved. In contrast, at temperatures above 450°C, nitrogen oxides were reported to promote the reaction and counteract long-term loss of methane conversion.[4,8] While this promotion has important advantages for the exhaust after-treatment, the high-temperature regime is expected to be rather difficult for studying surface intermediates due to negligible surface coverages. Therefore, this work will focus on the inhibition observed at low temperatures.

[a] Dr. A. Boubnov, Dr. A. Gremminger, Dr. M. Casapu, Prof. O. Deutschmann, Prof. J.-D. Grunwaldt
Institute for Chemical Technology and Polymer Chemistry
Karlsruhe Institute of Technology
Engesserstraße 20
76131 Karlsruhe (Germany)
E-mail: alexey.boubnov@kit.edu
        grunwaldt@kit.edu
Homepage: https://www.itcp.kit.edu/abgaszentrum/english/
          https://www.itcp.kit.edu/grunwaldt/english/
          https://www.trackact.kit.edu/

ChemCatChem

Research Article
doi.org/10.1002/cctc.202200573

Chemistry Europe
European Chemical
Societies Publishing

At temperatures below 700 °C where palladium oxide is stable against auto-reduction,[9] minor redox changes of palladium are difficult to observe, making redox-sensitive characterization ineffective.[8] Only above 750 °C palladium undergoes a reduction of PdO to metallic Pd, that can be detected by X-ray absorption spectroscopy (XAS), X-ray diffraction (XRD), Raman spectroscopy and thermal gravimetric analysis.[10] Furthermore, no changes of the PdO structure to e.g. formation of bulk hydroxides have been reported. Considering the low stability of hydroxide[11] or nitrite/nitrate[12] species, exposure of the catalyst in the temperature range of 200–450 °C to water or NO, respectively, is expected to lead mainly to surface structural changes, requiring surface-sensitive techniques to detect them. Typical bulk techniques such as XAS and XRD can suffer from severe limitations in detecting surface-confined structural transformations, which do not involve a change in oxidation state. On the other hand, surface-sensitive techniques like X-ray photoelectron spectroscopy (XPS) or total-electron-yield XAS, that are required to operate in the millibar pressure-regime or lower, are not suitable to probe the catalyst in its working state since the low pressure, among other factors, lowers the auto-reduction barrier of Pd.[13] Finally, surface-sensitive infrared spectroscopy is not element-specific and does not unambiguously identify the bonding site of the infrared-active molecule.

Hence, detection of purely surface-borne species on PdO during reaction at ambient pressure should be measured by element-specific techniques with enhanced surface-sensitivity. One approach towards improved sensitivity is the use of modulation-excitation spectroscopy (MES). In this technique, the chemical environment of the sample is modulated, or periodically alternated, and the structural dynamics mostly due to the changing surface species stimulated by the modulations are filtered from the background of static spectator species and noise. MES is versatile for studying reversible dynamics of catalysts with high sensitivity. This method was successfully used to reveal subtle changes between the metallic and oxide phases of exhaust-gas catalyst surfaces using XAS[14] and XRD,[15] barely detectable sulfur-oxygen exchange in promoted MoS₂-based hydrotreating catalysts,[16] oxygen functionalization and vacancy formation in IrO₂-based oxygen evolution electrocatalysts,[17] and dynamics in bimetallic methanation catalysts,[18] studied using XAS. The modulation-excitation method, likewise applied to infrared spectroscopy,[19] is suitable for probing the dynamic change of strongly adsorbed surface species on a catalyst surface, revealing the reaction mechanism.

In order to investigate the nature and location of the surface species involved in the inhibition of methane oxidation, we applied the MES approach complementary to *operando* XAS. Any detected structural changes were expected to originate from ligand interaction of the noble metals rather than their redox change, making them very small and the measurement especially challenging. The objective was to investigate the interaction of the reactants and inhibitors, H₂O and NO, during reaction with the noble metal component on bimetallic Pd–Pt/Al₂O₃, as well as monometallic Pd/Al₂O₃ model catalysts. Element-specific X-ray absorption spectroscopy in the more surface-sensitive modulation-excitation mode (ME-XAS) was used to probe the electronic structure of the two noble metals during periodic injection of trace methane to an oxygen-rich atmosphere and injecting inhibiting agents (H₂O, NO) to the lean methane-oxygen mixture. In this manner, the chemistry of the noble metal component during reaction and deactivation was to be uncovered. In addition, diffuse-reflection infrared Fourier-transform spectroscopy (DRIFTS) was used to probe the molecular species on the catalyst surface under these transient conditions. Since DRIFTS is not element-specific, experiments with the supported noble metal as well as with the support alone were used to shed light on which components are important for reaction and inhibition.

Results and Discussion

Palladium oxide with platinum doping on Al₂O₃ support

TEM images of 2.4% PdPt$_{0.1}$/Al₂O₃ and 2.4% Pd/Al₂O₃ (in the following Pd–Pt/Al₂O₃ and Pd/Al₂O₃ respectively), with a corresponding particle size distribution for the former, are shown in Figure 1 (a), (b) and (c). The mean noble metal nanoparticle size was determined as 2.6 ± 0.7 nm for the bimetallic, while the monometallic was very similar, with a minor fraction of larger nanoparticles up to maximum 10 nm. A very weak broad PdO(112) reflection at 55° can be observed in the XRD patterns in Figure 1 (d) and inset, indicating a low concentration of crystallites on the few-nanometer scale.
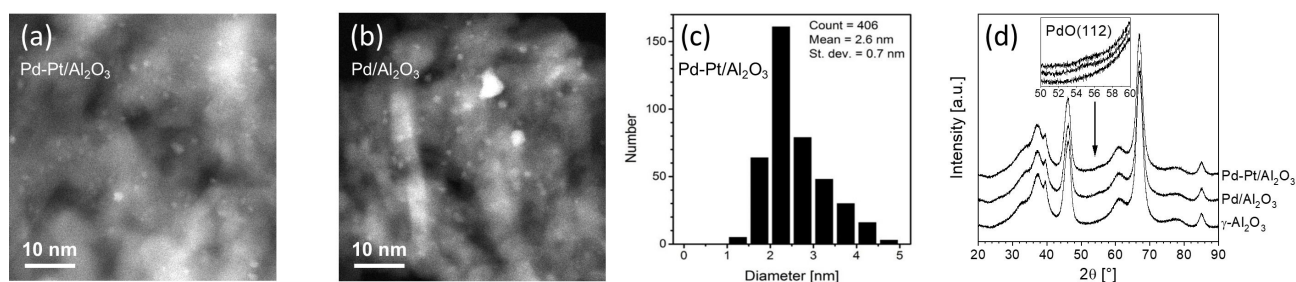
**Figure 1.** STEM images of (a) Pd–Pt/Al₂O₃ and (b) Pd/Al₂O₃, and (c) particle size distribution of Pd–Pt/Al₂O₃. (d) XRD pattern of the bimetallic and monometallic catalysts and pure Al₂O₃-support; inset shows the detail of the PdO(112) reflection.

ChemCatChem

Research Article
doi.org/10.1002/cctc.202200573

Chemistry
Europe

European Chemical
Societies Publishing

Metallic phases were not detected, as characteristic reflections of e.g. Pt(311) at 80.1° were absent.

The XANES results at the Pd K-edge shown in Figure 2 (a) indicate that the Pd component in both the Pd–Pt/Al_2O_3 and the Pd/Al_2O_3 catalysts were fully oxidized, i.e. in PdO stoichiometry. The corresponding EXAFS results depicted in Figure 2 (c), Figure S1 and Table 1 confirmed that the Pd component was in

the PdO phase. This was characterized by identical back-scattering paths for the nearest-neighbor Pd–O shell (2.02–2.03 Å) and further Pd–Pd shells (3.07 Å and 3.45–3.47 Å).

The Pt component in Pd–Pt/Al_2O_3 was highly oxidized like the PtO_2 reference, that is, O/Pt = 1.8 and 2.0 respectively, according to XANES in Figure 2 (b) and Table 1. For the local structure of Pt, EXAFS analysis was carried out at the Pt L_3-edge
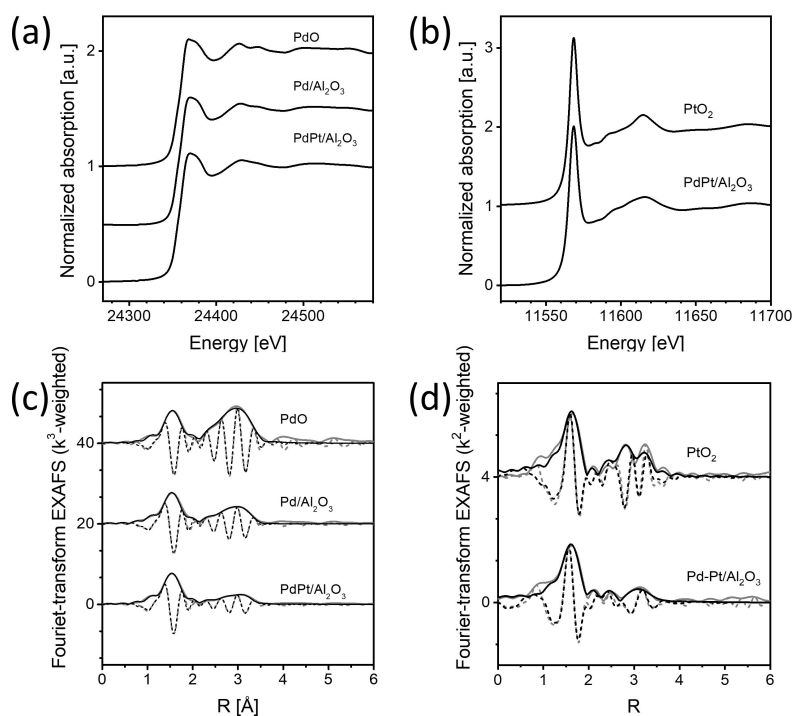
Figure 2. XANES spectra of Pd–Pt/Al_2O_3 and Pd/Al_2O_3 catalysts with reference oxides at the (a) Pd K-edge and (b) Pt L_3-edge. (c) and (d) are corresponding Fourier-transform EXAFS spectra (magnitude and imaginary part) with reference metal oxides for comparison. Grey: experimental data, black: fit. EXAFS spectra and fits in k-space are provided in Figure S1.

Table 1. Interatomic distances and coordination numbers determined by EXAFS analysis of the 2.4 % Pd/Al_2O_3 and 2.4 % Pd–Pt/Al_2O_3 catalysts and reference oxides at the Pd K-edge (Pd-x paths) and the Pt L_3-edge (Pt-x paths). Electronic amplitude reduction factors determined from metal foil spectra: $S_0^2 = 0.78 \pm 0.04$ for Pd K-edge and 0.77 ± 0.04 for Pt L_3-edge (Figure S2 and Table S1). Fitting space for all: k-range 3.0–12.5 Å^{-1}, R-range 1.0–3.7 Å, $N_{Nyquist} = 16$.

Sample	Path	d [Å]	CN	σ^2 [Å^2]	ΔE_0 [eV]	R-factor [%]
PdO	Pd–O	2.03 ± 0.01	3.9 ± 0.3	0.002 ± 0.001	0.4 ± 1.1	0.6
O/Pd = 1.0	Pd–Pd	3.07 ± 0.01	5.3 ± 1.2	0.005 ± 0.002		
	Pd-Pd	3.47 ± 0.01	4.7 ± 1.5	0.004 ± 0.002		
Pd/Al_2O_3	Pd–O	2.02 ± 0.01	3.9 ± 0.3	0.002 ± 0.001	-1.0 ± 1.2	0.9
O/Pd = 1.0	Pd–Pd	3.07 ± 0.02	3.1 ± 1.8	0.007 ± 0.004		
	Pd-Pd	3.45 ± 0.01	4.5 ± 2.7	0.008 ± 0.005		
Pd–Pt/Al_2O_3	Pd–O	2.02 ± 0.01	3.8 ± 0.3	0.002 ± 0.001	-0.5 ± 1.1	1.3
O/Pd = 1.0	Pd–Pd	3.07 ± 0.02	1.6 ± 0.8	0.006 ± 0.004		
	Pd-Pd	3.45 ± 0.02	2.9 ± 0.6	0.008 (fixed)		
Pd–Pt/Al_2O_3	Pt–O	1.99 ± 0.01	5.1 ± 0.6	0.002 ± 0.001	9.2 ± 1.2	4.2
O/Pt = 1.8	Pt–Pd	3.04 ± 0.02	4.3 ± 1.3	0.010 (fixed)		
	Pt-Pd	3.52 ± 0.05	2.9 ± 2.0	0.010 (fixed)		
PtO_2	Pt–O	2.02 ± 0.01	6.1 ± 0.8	0.003 ± 0.002	11.7 ± 1.0	3.6
O/Pt = 2.0	Pt-Pt	3.11 ± 0.01	10.0 ± 3.2	0.005 ± 0.002		

ChemCatChem

Research Article
doi.org/10.1002/cctc.202200573

Chemistry Europe
European Chemical
Societies Publishing

in Figure 2 (d) and Table 1, identifying the first Pt–O shell close to that in PtO_2, but with coordination number of ~5 instead of 6. The further coordination shells correspond fully to the structure in PdO, clearly indicating that the Pt atoms were incorporated into the PdO matrix at lattice positions of Pd atoms. The low coordination numbers observed in the catalysts relative to the bulk structures of PdO and PtO_2 showed low crystalline order, extending to only a few nanometers.

Using CO chemisorption, a dispersion of 40% was determined on both Pd/Al_2O_3 and $Pd–Pt/Al_2O_3$ catalysts, confirming on average 3 nm noble metal particles, which was in line with the TEM results. The high dispersion was important to achieve for studying surface effects under reaction conditions, especially using XAS, which probes all metal atoms without discriminating them by location. The total surface area of the noble metal per gram of catalyst was approximately 4.5 m^2/g, corresponding to 2.5% of the total BET surface area of 180 m^2/g. Based on this, it was expected that DRIFTS will be detecting a substantial amount of surface species on the Al_2O_3 surface besides those on the noble metal. Hence, a combination of DRIFTS with ME-XAS was considered essential for a holistic view on the surface chemistry.

Catalytic performance of methane oxidation without and with water and NO

Light-off curves measured in the lab-scale reactor under dry conditions of 3200 ppm $CH_4 + 10\%$ O_2 in balance N_2, Figure 3 (a) and (b), show similar performance of the $Pd–Pt/Al_2O_3$ and Pd/Al_2O_3 systems respectively. The light-off temperature T_{50} with 50% conversion during heating and cooling was approximately 310°C, showing a small inverse hysteresis. The addition of 12% water vapor (grey curves) caused T_{50} to increase to ca. 420°C, observing the same inverse hysteresis. We explain the inverse hysteresis with auto-inhibition of the catalyst by water produced directly on the catalyst surface at full conversion.[20]

In the capillary reactor, Figure 3 (c) and (d), the light-off temperature was also 310°C, but after reaching just above 500°C, T_{50} decreased to approximately 270°C during cooling down, demonstrating a regular hysteresis known for e.g. CO oxidation.[21] This opposite behavior in comparison to the lab reactor is most probably due to the reaction exothermicity combined with the use of an undiluted catalyst bed for the spectroscopic investigations, leading to slightly different heat and mass-transport properties, cf. Figure 3 (a, b) and (c, d). The addition of 200 ppm NO to the gas flow in repeated measurements (grey curves) decreased the conversion, maintaining the hysteresis, but to a lesser extent.
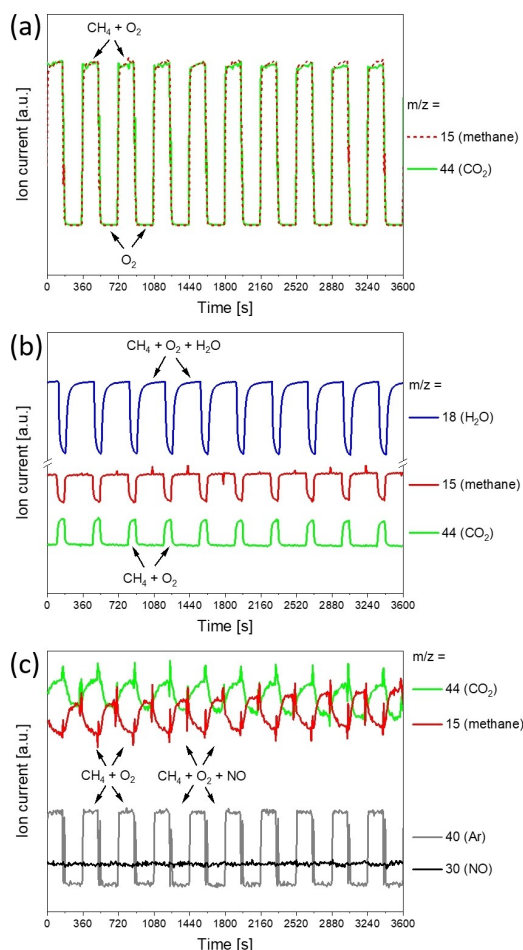
The modulation-excitation X-ray absorption spectroscopy (ME-XAS) experiments (*vide infra*) were conducted at an
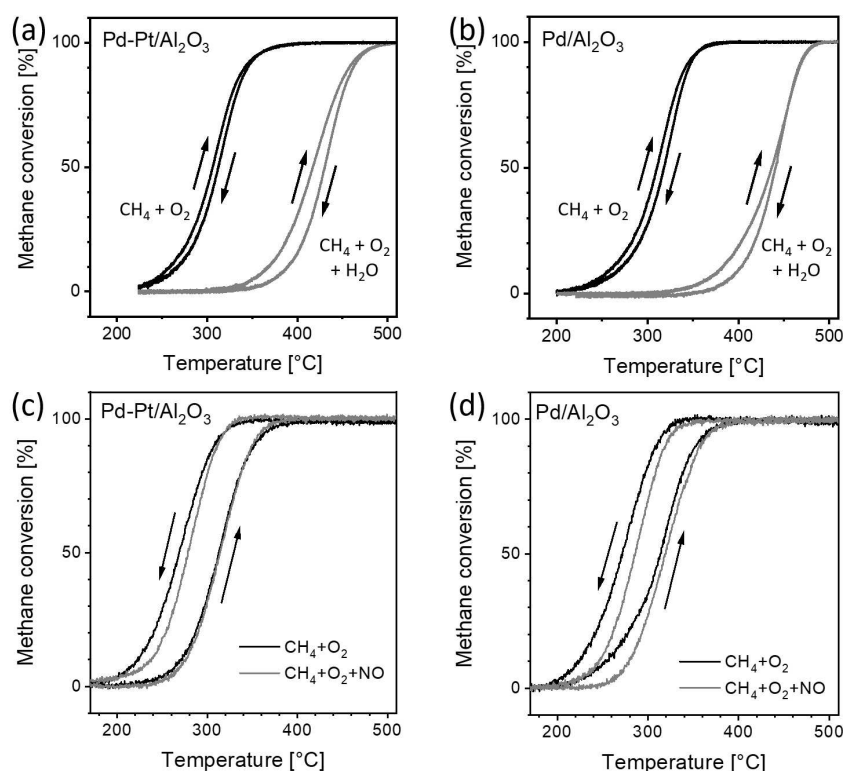
Figure 3. Light-off curves for methane oxidation over (a, c) 2.4% $Pd–Pt/Al_2O_3$ and (b, d) 2.4% Pd/Al_2O_3 during heating and cooling with and without the presence of (a, b) H_2O and (c, d) NO. (a, b) was measured in a 8 mm quartz laboratory reactor; gas composition: 3200 ppm $CH_4 + 10\%$ O_2 (+12% H_2O), balance N_2, total flow 1 L/min, temperature ramp 3 K/min. (c, d) was measured in a 3 mm quartz capillary used for subsequent XAS studies; gas composition: 4000 ppm $CH_4 + 10\%$ O_2 (+200 ppm NO), balance He, total flow 50 mL/min, temperature ramp 5 K/min.

ChemCatChem

Research Article
doi.org/10.1002/cctc.202200573

Chemistry Europe
European Chemical
Societies Publishing

isothermal T_{50}, which was found by varying the temperature until methane conversion of 50% under dry conditions was reached and stabilized. In this regime, the changes in methane conversion were best measurable. This temperature point could vary by several tens of degrees depending on the sample type and unavoidable small variations in the catalyst mass during different *operando* measurements. The T_{50} was chosen as the operating temperature since at this point the strongest activity variation during addition of inhibition agents could be obtained; important in all cases was that the temperature was below 450 °C, a point where adsorption of inhibiting agents is negligible for the inhibition to play a role.

The first experiment studied the effect of methane cut-off at $T_{50} = 302$ °C, in a methane-oxygen mixture (4000 ppm $CH_4 +$ 10% O_2 in balance He), and the results are reported in Figure 4 (a). Upon methane cut-off retaining an oxygen-only mixture (10% O_2 in balance He) both methane and CO_2 immediately disappeared from the gas flow. In the second experiment, the addition of 1% H_2O, Figure 4 (b) to the dry $CH_4 + O_2$ gas mixture caused a rapid decrease of methane conversion, which was

promptly recovered when water vapor was removed. Noteworthy is that the water-containing cycle was somewhat longer than the water-free cycle due to the lack of heat-tracing on the gas lines and therefore longer time necessary to stabilize the gas atmosphere in the *operando* setup. In the third experiment, the addition of 200 ppm NO, Figure 4 (c), likewise caused a reversible decrease of methane conversion. NO is poorly detected by mass spectrometry, therefore argon was used in the NO-free mixture to trace the switches.
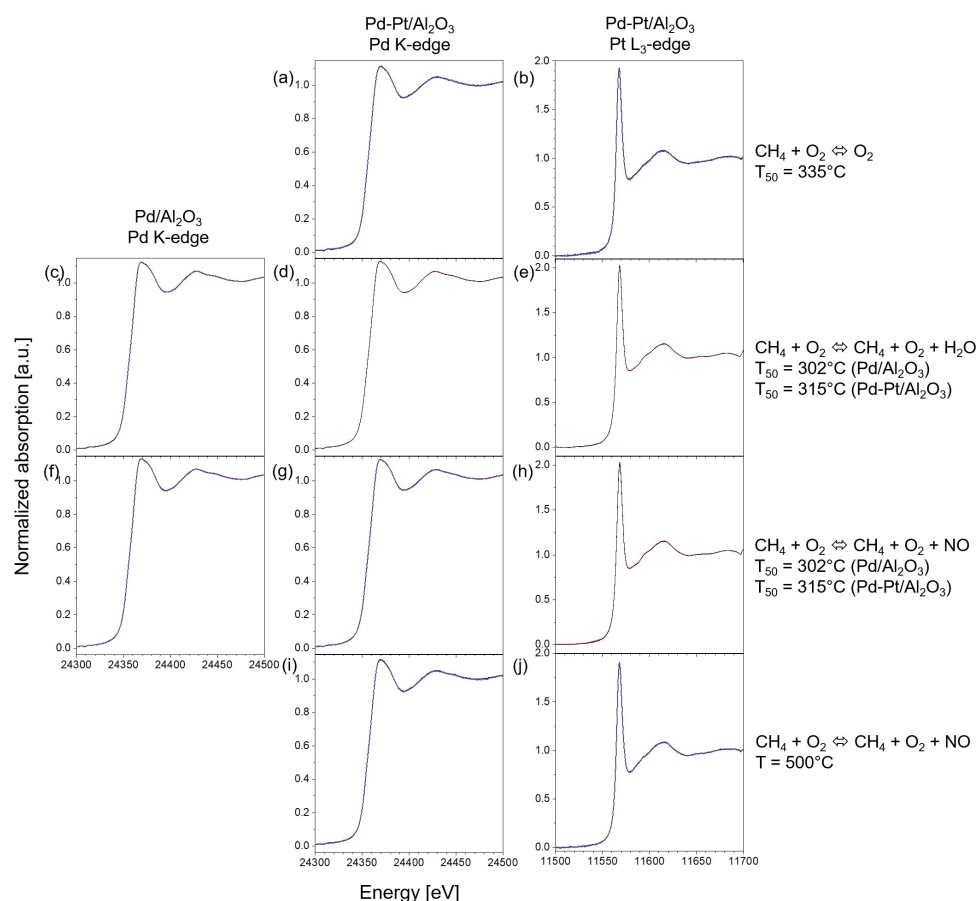
Important is to note that the inhibition was reversible, as the conversion immediately increased once the inhibiting molecule was removed, which is an important pre-requisite for modulation-excitation experiments. However, with every subsequent cycle, the methane conversion slightly decreased in all three experiments, indicating a long-term deactivation, which is outside of the scope of this paper.

Time-resolved and phase-resolved XANES spectroscopy

During all three experiments, the time-resolved XANES spectra showed completely oxidized Pd and Pt during both initial and inhibited reaction conditions with no detectable changes, as illustrated in Figure 5. The displayed time-resolved XANES spectra represent 3 minutes in the initial reaction mixture plus 3 minutes under inhibited reaction conditions (methane cut-off, water or NO addition), averaged over 10–15 periods (total of 36 spectra) into one single 6 minute period. This procedure significantly increased the signal-to-noise ratio. The spectra are overlapped, and detail views of the edge maximum are displayed in Figure S3, to emphasize that the variations even in this strongest feature were infinitesimal and affected by noise, requiring the examination of the full XANES spectrum with high sensitivity.

In order to enhance any electronic changes contained in the XANES spectra, the modulation-excitation method was applied. The time-resolved XANES spectra were demodulated into phase-resolved spectra by applying a first-order Fourier-filter, i.e., a sine function of a 6-minute period with phase shifts ($\Delta\phi$) between 0° and 360° analogous to,[16a] Figure 6. The maximum component was found to be at or close to $\Delta\phi = 0°$, indicating that the spectral response of both the Pd K and Pt L_3-edges to the changing reaction mixtures was immediate at T_{50}, directly following that of the methane conversion.

In fact, the demodulated spectra at $\Delta\phi = 0°$ can be thought of as differences "XANES under reaction conditions minus XANES under inhibiting conditions", so an alternative way of evaluating the data is taking the difference of these respective XANES spectra. Nevertheless, the demodulation using a sine filter effectively used all data, resulting in a higher-quality spectrum, whereas merely taking a spectral difference of the extreme states significantly decreasing the quality; a comparison of both data treatments with the same time-resolved dataset is presented in Figure S5. In the context of the magnitude of the demodulated spectra, we note that no transfer function or correction terms were used here to take into account the shape of the spectral response. To check that

Figure 4. Mass spectrometer signals over 10 periods of gas modulation over Pd–Pt/Al_2O_3: (a) $CH_4 + O_2 \leftrightarrow O_2$ at $T_{50} = 335$ °C, (b) $CH_4 + O_2 \leftrightarrow CH_4 + O_2 + H_2O$ at $T_{50} = 315$ °C and (c) $CH_4 + O_2 \leftrightarrow CH_4 + O_2 + NO$ at $T_{50} = 315$ °C. Gas concentrations in balance He: 4000 ppm CH_4, 10% O_2, 1% H_2O, 200 ppm NO, total flow 50 mL/min in a 3 mm quartz capillary.

Figure 5. Time-resolved Pd K-edge and Pt L$_3$-edge XANES spectra during cycles of (a–b) methane on/off, (c–e) water off/on and (f–j) NO off/on over Pd/Al$_2$O$_3$ and Pd–Pt/Al$_2$O$_3$ as indicated, at indicated temperatures. Displayed are spectra with 10 second intervals in the averaged modulation period. The changes are not visible or significantly distinguishable even when zooming in, cf. Figure S3.

the shape of the spectral response to the modulation can sufficiently be represented by the sine function, we plotted the temporal evolution of selected maxima and minima of the time-resolved XANES spectra in the averaged 6-minute period, with overlaid $\pm \sin(t)$, in Figure S4. As seen from the plots, a weak and relatively smooth sinusoidal trend can be observed for most of the plots; we note that the actual phase-resolved spectra were calculated using all data points of the time-resolved XANES, serving as a sound reason to justify that the resulting phase-resolved spectra contain real spectral features. For comparison, Figure 6 (i, j) is completely missing identifiable spectral features. Hence, the plain sine function was deemed accurate enough for extracting the spectral features and using them further for comparison with simulated spectra, as will be described below.

The following sections deal with theoretically calculated XANES spectra, their differences spectra, and how they were used to qualitatively interpret the minute structural changes of the catalyst detected by ME-XAS.

Models of Pd and Pt centers and their simulated XANES

Complementary to the experimental ME-XAS, we simulated using the FEFF9-code XANES spectra of the Pd and Pt centers in hypothetical chemical environments expected during the ME-XAS experiments. The differences between various pairs of simulated XANES were interpreted by matching them with experimental ME-XANES and the most alike spectra with the most probable chemical environment were proposed.

The models of the Pd centers were based on the PdO crystal lattice (space group $P\,4_2/m\,c$), containing the central Pd atom on the PdO(100) plane. Pd exists in PdO$_4$ plane-rectangular moieties, close to square geometry. PdO$_4$-moieties facing the (100) direction are stacked and share O-corners with stacked PdO$_4$-moieties that are facing the (010) direction. The models built here consisted of a central (010)-facing PdO$_4$-moiety surrounded by three moieties of the same orientation, two stacking one on each side, as well as one sharing two O-corners with the central. In this way, these plane rectangular moieties were "standing" on the terminating (100) plane. Four further (100)-facing PdO$_4$-moieties connected the ensemble of the (010)-facing PdO$_4$-moieties, by sharing O-corners, into a single crystal, as depicted in Figure 7 (d) labelled "PdO$_2$". This name
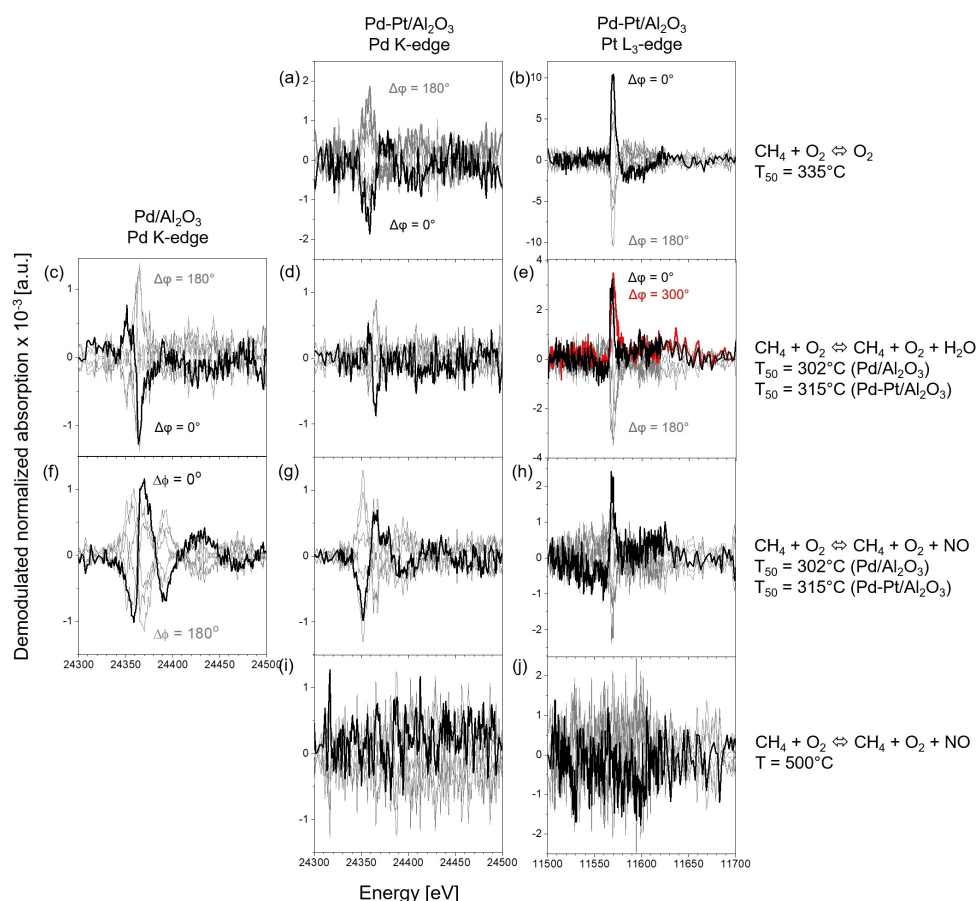
Figure 6. Phase-resolved Pd K-edge and Pt L$_3$-edge XANES spectra corresponding to Figure 5 during cycles of (a-b) methane on/off, (c–e) water off/on and (f–j) NO off/on over Pd/Al$_2$O$_3$ and Pd–Pt/Al$_2$O$_3$ as indicated, at indicated temperatures. Displayed are spectra incremented by 10° demodulated phase angle, black lines indicate in-phase signal ($\Delta\phi = 0°$); out-of-phase ($\Delta\phi = 180°$) is the signal with the opposite sign.
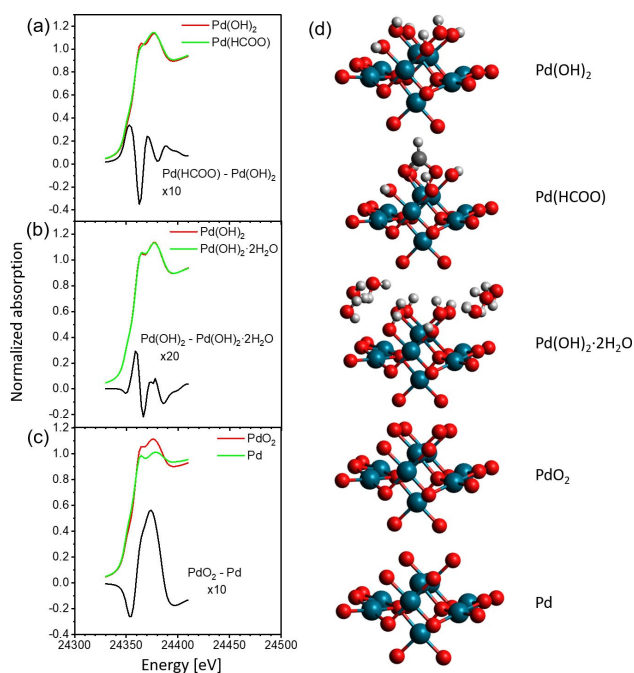
refers to the Pd central atom with 2 oxygens extending from the surface, which were the only variable atoms in the models, surrounded by a non-varying environment mimicking the PdO(100) surface. Removing the two oxygens left "Pd", a bare Pd atom bound to the crystal, whereas modification of these coordination sites with hydroxyl groups, coordinating water molecules, formate, nitrate, nitrite and nitrosyl groups yielded corresponding 10 structures, named "Pd(OH)$_2$", "Pd(HCOO)" etc., as depicted in Figures 7 (d) and S8.

Models of Pt centers incorporated in a Pd(100) surface were built based on the Pd model, but the stack of the central (010)-facing PdO$_4$ moiety with two such further moieties on each side was replaced by a single octahedrally-coordinated PtO$_6$ moiety with the two additional oxygens extending in the directions where the two PdO$_4$ moieties were removed. The structures were modified with the same ligands as for the Pd centers, resulting in 26 models, named "PtO$_4$", "Pt", "Pt(OH)$_4$" etc., relating to the variable functionalities on the four coordination sites of Pt. The structures are shown in Figures 8 (d) and S9.

All structures were relaxed in a Universal force field using the Avogadro program, as described in the Experimental Section. Pd K-edge and Pt L$_3$-edge XANES spectra were calculated of the central Pd and Pt atoms, and difference-XANES

spectra were calculated relative to a reasonable reference state, e.g. "Pd(HCOO)" – "Pd(OH)$_2$" represents the substitution of formate ligands by hydroxyls on Pd hypothesized during switches from a dry to a wet reaction mixture. Selected structures and corresponding difference-XANES most closely resembling the experimental data are shown in Figures 7 and 8, while all structural models with spectra, representing mixed ligands, and having many similarities with the former, are presented in Figures S8 and S9.

Note that a direct comparison of simulated data with experimental data requires a reliable simulation in terms of the intensities and energy-positions of the spectroscopic features. In order to back up the reliability of the feature intensities, used in the following sections for estimating the number of participating atoms, we conducted a benchmarking of the simulation of spectra of bulk reference compounds: PdO, Pd, PtO$_2$ and Pt, shown in Figure S6. We found that the white line intensity for bulk PdO is ca. 1.2 in experimental XANES and ca. 1.1 in the FEFF-simulation. For PtO$_2$, the experiment shows an intensity of about 2.1 and simulation of about 1.8. The XANES spectra of metallic Pd and Pt are also reliably simulated, but are of less relevance since the catalyst models used are oxide-based. Based on these results, we can conclude that FEFF

ChemCatChem

Research Article
doi.org/10.1002/cctc.202200573

Chemistry Europe
European Chemical
Societies Publishing

Figure 7. Calculated Pd K-edge XANES (FEFF9) of most likely model structures and difference spectra for comparison with phase-resolved XANES. Color legend: blue, Pd; red, O; white, H; grey, C. All model structures and Pd K-edge spectra are shown in Figure S8.
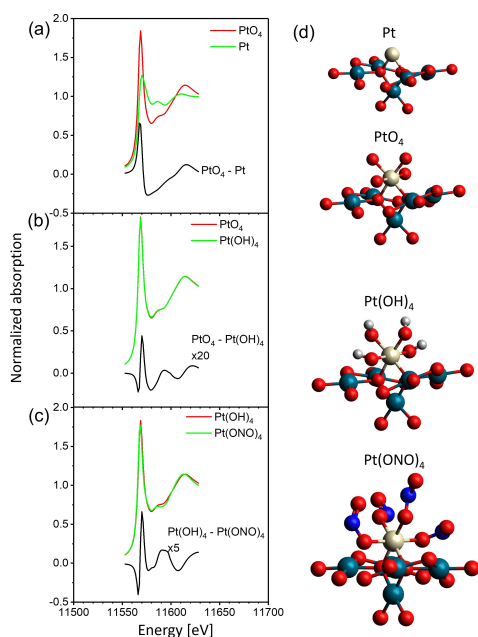
Figure 8. Calculated Pt L$_3$-edge XANES (FEFF9) of most likely model structures and difference spectra for comparison with phase-resolved XANES. Color legend: beige, Pt; blue, Pd; red, O; white, H; grey, C. All model structures and Pt L$_3$-edge spectra are shown in Figure S9.

systematically under-estimates the absolute white line intensities, and simulated spectra of the model catalysts, discussed in the following sections, exhibit similarly under-estimated white line intensities in the highest oxidation state. Based on this

systematic comparison, we consider the magnitudes of the difference-spectra suitable for direct comparison with the demodulated XANES. Based on this comparison also with respect to the positions of the prominent features, we also assume that the shapes of the difference-spectra can also be considered trustworthy, as the structures used for difference-spectra are similar with only ligands changing.

Effect of methane cut-off

During the experiment with methane cut-off on the Pd–Pt/Al$_2$O$_3$ system, both the palladium and platinum phases remained fully oxidized, as mentioned in sections above and seen in the Pd K-edge and Pt L$_3$-edge XANES spectra in Figure 5 (a) and (b). In the phase-resolved Pd K-edge XANES in Figure 6 (a), in-phase demodulated spectra ($\Delta\phi = 0°$) exhibited the largest variation, showing that the structural changes were synchronous with the gas modulation; the same with the opposite sign was observed out-of-phase ($\Delta\phi = 180°$). This variation was a feature characterized by a minimum at 24355–24360 eV, followed by a small maximum. Relative to the time-resolved XANES this was a decrease in the edge onset, before the main maximum. The difference between simulated spectra of "Pd(HCOO)" and "Pd(OH)$_2$" in Figure 7 (a) showed similar features, however with some deviation from the experimental data. This difference represents the presence of formate groups on the Pd during reaction, as will be shown with DRIFTS later, and their replacement with hydroxyl groups during methane cut-off. Among all the generated difference spectra shown in Figure S8 this was the closest resemblance, although it cannot be excluded that other processes or their combinations were also taking place.

In the corresponding in-phase Pt L$_3$-edge XANES, a narrow intense maximum at 15560 eV followed by a broad minimum occurred, shown in Figure 6 (b). This spectral difference closely resembled the difference "PtO$_4$" and "Pt", meaning that each methane cut-off caused the segregation of oxygen-stripped Pt from the Pt:PdO solid solution during the switching. Furthermore, there is strong resemblance to the difference of the spectra between bulk PtO$_2$ and metallic Pt as shown in Figure S7 (b), indicating that the bulk transformation of the oxide to metal is electronically analogous to the stripping of surface oxygens.

This finding was contradictory to our expectations given that the methane-free gas blend was more oxidizing than the methane-containing, and nevertheless was evidence of transformations of the catalyst or redox-related interplay between Pd and Pt that need to be studied further by advanced techniques. In general, the fact of the role of metallic Pt as promoter of the PdO methane oxidation catalyst is well-known,[22] but the fundamental reason is yet to be clarified.

At this point, we made efforts to quantify the participating sites by taking the ratio of the amplitudes of the strongest feature in the experimental ME-XANES at $\Delta\phi = 0°$ and the corresponding theoretical difference-XANES. The results are presented in Supplementary Notes and Table S2. When compar-

ChemCatChem

Research Article
doi.org/10.1002/cctc.202200573

**Chemistry
Europe**
European Chemical
Societies Publishing

ing the amplitude of the XANES features in the demodulated spectra (showing only the spectral changes of the participating Pd and Pt sites) to the simulated difference spectra (assuming all Pd and Pt sites are involved), we note that the former is systematically lower than the latter. This means that only a fraction of the Pd and Pt sites were involved in the reaction at the same time, which is also the case in the following experiments with inhibition by water and NO (*vide infra*). However, we consider an explicit quantification and assignment of the participating sites only preliminary, as the spectral amplitudes are burdened by errors originating from the lack of a transfer function, which takes into account the shape of the modulation stimulus and response, as well as the kinetics, as discussed in ref..[23] For a reliable quantification, a more rigorous treatment on data of better quality is required; therefore, we focus here only on the qualitative analysis.

Effect of inhibition by H_2O

When water vapor was periodically added to and removed from the gas stream, bulk changes to the catalyst structure were not detectable by conventional XAS; experiments were done both with monometallic Pd/Al_2O_3 and bimetallic $Pd–Pt/Al_2O_3$ as shown in Figure 5 (c–e). Reversible spectral changes were however seen in the phase-resolved spectra. The in-phase Pd component of both the monometallic Pd/Al_2O_3 and bimetallic $Pd–Pt/Al_2O_3$ seen in Figure 6 (c–d) consistently shows a sharp minimum at 24365 eV surrounded by other features: a maximum at 24350 eV plus a negative shoulder at 24380 eV for Pd/Al_2O_3 and a small maximum at 24355 eV for $Pd–Pt/Al_2O_3$.

Qualitatively, these features, especially the minimum, are characteristic for at least two chemical changes when examining the calculated difference-XANES. One possibility is the exchange of formate by hydroxyl groups as in methane cut-off where self-inhibition of the reaction by product water occurs, Figure 7 (a). Another possibility is the change between models "$Pd(OH)_2$" and "$Pd(OH)_2 \cdot 2H_2O$" (Figure 7 (b)), here demonstrating the hydration of the already existing hydroxyl groups, also inhibiting the reaction. Commonly, water adsorption is speculated to cause hydroxylation of the palladium oxide surface, inhibiting methane oxidation;[24] this calculated difference-XANES suggests that merely the interaction of water modifies the electronic structure of the noble metal surface, which may likewise be a deactivation mechanism.

The phase-resolved XANES of Pt at and close to in-phase angles ($\Delta\phi = 0°$, 300°) shown in Figure 6 (e) exhibit a sharp maximum at the position of the white line, preceded by a small minimum, which corresponds to a decrease of the white line height and a slight shift to lower energy during the water-containing half-cycle. Simulated XANES spectra of Pt shown in Figure 8 (b) demonstrate that such a spectral change can be caused by hydroxylation of the oxo groups on the Pt centers. In fact, also difference-XANES of formate groups replacing hydroxides caused similar spectral changes (Figure S9 (e-g)), and this seemingly contradictory scenario during addition of water vapor is interesting to further investigate, since formate

adsorption on Pt is stronger than on Pd, as determined for formic acid oxidation electrocatalysis.[25]

The measurable response of both Pd and Pt during water inhibition suggests that a significant portion of the noble metal surface was structurally altered. Hence, the selected structural models for XANES calculations were deemed representative of the local catalyst structure in the light of theoretical work on unsupported PdO systems.[26] On the other hand, the use of supported catalysts and a high metal dispersion, as in our case, is ideal for experimentally probing the noble metal surface by XAS.

Furthermore, the participation of both metals suggests that the two elements were homogeneously distributed in the nanoparticles and exhibited no preference to be at the surface. This indifference can be assigned to the fully oxidized state of especially Pt. In contrast, the monometallic Pd/Al_2O_3 catalyst has shown the same response to water as the bimetallic, cf. Figure 6 (c, d); hence Pt does not act in the stabilization of the catalyst in the oxidized state and a certain degree of reduction is required for gaining full advantage of Pt addition.[22b] Under the oxidizing conditions of the present experiments, fully oxidized Pt is probably not a promoter but a passive participant of the surface reaction, as the intrinsic activity of Pt in the given temperature range is very low,[22a,b] and no segregation of Pt towards the core of the particles was observed as in the case where Pt is reduced to the metallic state.[8,27] Hence, Pt can here be regarded as an alternative probe of the interaction of the reactants with the catalyst surface, and its exact role may be clarified further in a promoter-test, similar to that reported for Bi-doped Pd- or Pt-catalysts during alcohol oxidation.[28]

Effect of inhibition and activation by NO

Time-resolved XANES spectra during the NO inhibition experiment over Pd/Al_2O_3 and $Pd–Pt/Al_2O_3$ are shown in Figure 5 (f-h) and as in previous cases, the response of the noble metal components towards NO addition was hardly detectable.

Like in the previous experiments, the modulation-excitation method was successfully applied to detect these minute spectral variations. Phase-resolved Pd K-edge XANES spectra on Pd/Al_2O_3 and $Pd–Pt/Al_2O_3$ are shown in Figure 6 (f, g). Both spectra with the highest intensity at $\Delta\phi = 0°$ are roughly characterized by a maximum at 24370 eV with a high-energy shoulder, surrounded by minima at 24360 eV and 24390 eV.

These are completely different features than the ones observed with water inhibition, indicating that the MES method is not only highly sensitive, but also very specific to the chemical environment. The ME-XANES spectra were compared to calculated XANES spectra and their differences, and the broad peaks matched most closely with the difference "PdO_2" – "Pd" shown in Figure 7 (c), meaning that during NO addition, the palladium sites lose their oxo-ligands. Direct similarities were also observed to the difference between bulk PdO and metallic Pd as shown in Figure S7 (a), indicating that removal of surface oxygens can be modelled by bulk oxide-to-metal transformations, as in the case for Pt discussed for methane cut-

ChemCatChem

Research Article
doi.org/10.1002/cctc.202200573

Chemistry
Europe
European Chemical
Societies Publishing

off. Comparisons with nitrogen-bearing ligands such as nitrites in Figure S8 (f, g), nitrates in Figure S8 (h) or nitrosyls in Figure S8 (i, j) identified unique spectral signatures with narrow peaks, that however did not match the experimental data. The lack of detectable NO_x-interaction with Pd sites (on both Pd/Al_2O_3 and Pd–Pt/Al_2O_3) together with a surface-reduction suggests that palladium rapidly oxidizes NO from the gas phase, leaving an oxygen vacancy, consistent with a suggested mechanism.[29] However, given the low intrinsic activity of Pd towards NO oxidation,[30] the results suggest that the mechanism of methane oxidation in the presence of NO is a complex process to be investigated further.

Phase-resolved Pt L_3-edge XANES spectra shown in Figure 6 (h) have exhibited a maximum at 11570 eV, preceded by a broad dip at lower energies and followed by a broad maximum at higher energies, for $\Delta\phi = 0°$. In the calculated XANES and their difference-spectra, the same set of features were observed for both monodentate nitrite shown in Figure S9 (h-o) and bidentate nitrate ligands shown in Figure S9 (p-r), in different combinations with hydroxyl groups. For the sake of direct comparison with the experimental data, only the Pt fully coordinated by four monodentate nitrite ligands is shown in Figure 8 (c). This match between theory and experiment demonstrates the replacement of hydroxyls with nitrites or nitrates on Pt the during addition of NO, and emphasizes the active role of Pt in adsorbing and oxidizing NO to NO_2, being, unlike Pd, a well-suited catalyst for this reaction,[30] also consistent with the fact that the binding of NO is weak on Pd and strong on Pt.[31] The rapid conversion of NO was further witnessed by the lack of adsorbed NO, as none of the theoretical XANES spectra involving platinum nitrosyl complexes shown in Figure S9 (s-z) matched the experimental data. The qualitative differences between the ME-XANES spectra of the monometallic Pd/Al_2O_3 and bimetallic Pd–Pt/Al_2O_3 catalysts, comparing Figures 6 (f) and (g), suggest that some electron-transfer processes between Pd and Pt are taking place, but this is outside the scope of this work.

The addition of NO to the reaction mixture at 500°C when full methane conversion took place was also investigated. Both the time-resolved XANES of Pd and Pt shown in Figure 5 (i, j) showed no observable changes, and also the phase-resolved XANES of both metals shown in Figure 6 (i, j) were dominated by random noise with no distinguishable spectral features. As expected, stable adsorbates could not be detected at these high temperatures.

The following sections with DRIFTS will address the role of temperature for the surface adsorbates, also shedding light upon the role of the support during inhibition of methane oxidation.

Surface species during methane oxidation

Previous sections have demonstrated the role of the noble metal sites for methane oxidation and inhibition by water and NO. For a full picture of long-lived educts, intermediates and products on the cata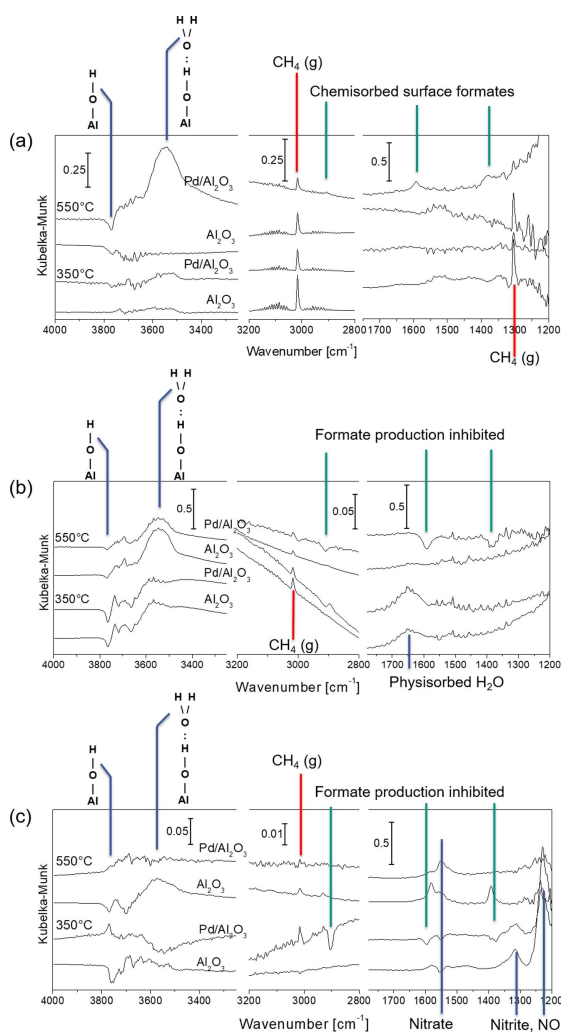lyst surface, including those on the alumina support, we turned to diffuse-reflectance infrared Fourier-transform spectroscopy (DRIFTS). Having deduced from XAS that fully oxidized Pt does not play a crucial role for methane oxidation, we simplified the DRIFTS study to the monometallic Pd/Al_2O_3 catalyst, and compared its behavior under reaction conditions to that of the bare Al_2O_3 support.

Under the dry reaction mixture (4000 ppm CH_4 + 10% O_2 in balance He), methane conversion was 100% at 550°C and 25% at 350°C on Pd/Al_2O_3, and always zero on Al_2O_3. Note that the conversion was integral conversion over a catalyst bed in the *in situ* cell with a strong temperature gradient of about 150 K between the circumference of the catalyst bed held at the reported setpoint temperature, and the center where the catalyst was probed with the infrared beam. This practically means that at 550°C, the center of the catalyst bed was in a working state (~400°C) and all observed surface species were relevant, but at 350°C, the temperature at the center was likely only sufficient for very low methane conversion.

After the dry reaction mixture was admitted to a baked-out catalyst or support at both temperatures, narrow bands at 3000 and 1300 cm^{-1} due to gas-phase methane[32] appeared, Figure 9 (a). At 550°C, broadened bands at 3000, 2900, as well as 1600 and 1400 cm^{-1} appeared, assigned to surface formate species formed as a result of adsorption and activation of methane, after which the complete oxidation reaction proceeds unhindered as reported previously.[26b] The presence of formate intermediates and water product was positively correlated with methane conversion. This finding also rules out the bicarbonate pathway suggested by theory,[33] as no characteristic bands for bicarbonates or carbonates were observed. Water produced in the reaction adsorbed on the alumina surface hydroxyls, giving rise to a broad band between 3500–3600 cm^{-1} (O–H stretch of the water molecule) and a small negative band at 3770 cm^{-1} (O–H stretch of the occupied surface hydroxyl of the alumina).[7a] Bands of adsorbed formates and water were previously reported on alumina-supported Pd, and to a much weaker extent on zeolite-supported catalysts,[34] making it reasonable to assume that a part of these molecules produced by methane oxidation on Pd are stored on the alumina support. The ME-XANES results above suggest that a some of the formate ligands are also present on palladium oxide, but in the present work it is not possible to differentiate the adsorption locations. None of these bands were observed on bare alumina or at 350°C, as methane was not activated to formate, and water was not produced as oxidation product.

Surface species during water inhibition

The effect of adding water vapor to the catalyst already running under the dry reaction mixture is shown in Figure 9 (b). The hydrogen-bond associated water band at 3500–3600 cm^{-1} and the corresponding negative hydroxyl band at 3770 cm^{-1} as described above were observed, corresponding to a high surface coverage by water of alumina, both as support for Pd and bare. Also at 350°C, a broad band at 1650 cm^{-1}, assigned to HOH-scissors vibration of physisorbed water[35] was observed

ChemCatChem

Research Article
doi.org/10.1002/cctc.202200573

**Chemistry
Europe**
European Chemical
Societies Publishing

Figure 9. Evolution of surface species detected by *in situ* DRIFTS on 2.4% Pd/Al$_2$O$_3$ catalyst and bare Al$_2$O$_3$ exposed to (a) methane + oxygen, (b) methanol + oxygen + water and (c) methane + oxygen + NO at 350°C and 550°C. DRIFT spectra are presented relative to spectra recorded under oxygen-only for (a) and methane + oxygen for (b) and (c). Gas component concentrations were 4000 ppm methane, 10% oxygen, 1% H$_2$O and 200 ppm NO in balance helium. The total flow was 200 mL/min.

adsorption of formates produced by dosing methanol or formic acid vapors.[26b]

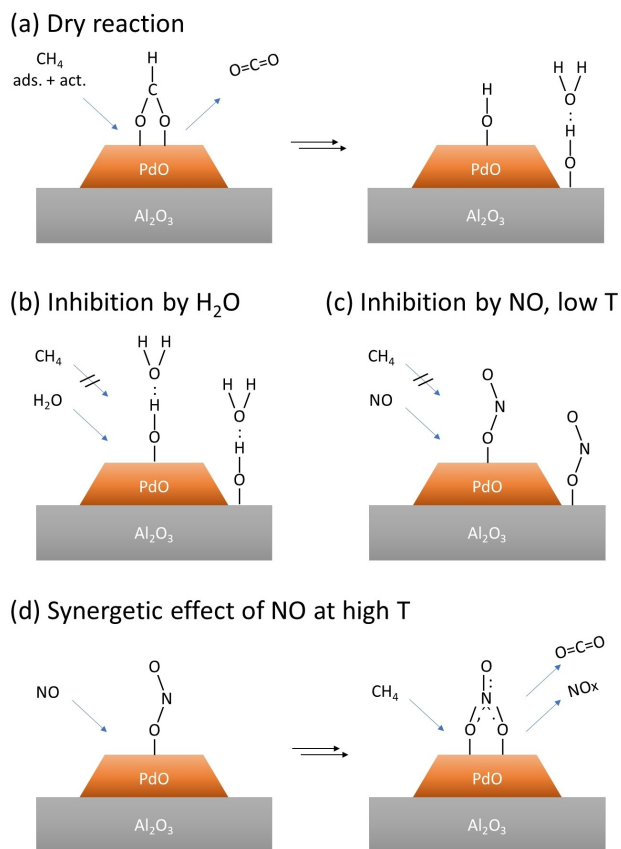## Surface species: inhibition and activation by NO

The effect of NO on the observed surface species was studied in an analogous manner as with water. The DRIFT spectra shown in Figure 9 (c) show the evolution of surface species when NO was added to the already running dry reaction mixture. At 350°C, NO was immediately adsorbed on both the catalyst and bare alumina as surface nitrite groups (1250 and 1320 cm^{-1})[36] without forming nitrosyl groups, as characteristic bands in the range 1800–2000 cm^{-1} were not observed,[37] in line with ME-XANES results ruling out NO adsorption on the noble metals. Hereby, the surface coverage of formates on Pd/Al$_2$O$_3$ decreased, as seen in the corresponding negative bands. The water production in the course of reaction was also inhibited, seen by the inverted bands from water at 3500–3800 cm^{-1}. The inhibition at 350°C indicated that methane oxidation was running before addition of NO, even if with a very low conversion.

At 550°C, instead of the nitrite bands, nitrate species at 1550 cm^{-1}[36a] were observed on Pd/Al$_2$O$_3$, indicating NO oxidation to NO$_2$. Under these conditions, no inhibition took place over the catalyst, as no negative formate bands were observed. This is an indication of a gas-phase reaction of methane with NO$_2$ to CO$_2$ and NO, which has also been reported previously[4] and which can explain the positive effect of NO$_x$ on methane oxidation above 450°C. On the other hand, positive bands corresponding to methane and formate species as well as H-bond associated water were observed for bare alumina, but could not be assigned to reasonable surface intermediates, as no reaction was expected to occur.

Proposed mechanisms for methane oxidation reaction and inhibition

Based on the combined findings of ME-XAS and DRIFTS, we here propose a mechanism during methane oxidation and deactivation for PdO nanoparticles supported on alumina. Figure 10 (a) shows schematically the methane activation and oxidation via the formate route on PdO, after which the produced water moves to the alumina support. Formate adsorption is important directly on the PdO surface, but its adsorption on the alumina support was not clarified.

Inhibition by externally applied water shown in Figure 10 (b) acts directly on the PdO particles surface as well as from the side of the alumina support onto the periphery of the particles, blocking the methane activation sites in the form of physisorbed water and hydroxyl groups. Inhibition by NO shown in Figure 10 (c) acts via adsorbed nitrites on the alumina support, likewise blocking methane activation, most likely from the periphery of the PdO particles, ME-XANES did not support the direct interaction of NO$_x$ with PdO. However, if Pt was present in the catalyst, it was found to interact with the NO$_x$ adsorbates.

on both catalyst and alumina. At 550°C on Pd/Al$_2$O$_3$, where methane oxidation was running, negative bands at 1400, 1600 and 2900 cm^{-1} corresponding to formate surface species appeared, indicating that their production in the course of the reaction was interrupted, and possibly displaced competitively by water molecules from their adsorption sites. Bare alumina did not show these changes, as the reaction did not proceed on it. Like above, it was not possible to distinguish between the adsorption sites of water and outcompeted formates between the noble metal and the support; combining the findings of DRIFTS with ME-XANES described above, adsorption should be able to take place on both. The competition itself between water and formate is also strongly dependent on factors such as the number of these competing molecules and their source; we have previously shown that water does not inhibit

Figure 10. Proposed mechanism of methane oxidation (a) under water-free conditions, (b) inhibited in presence of water at 50% conversion, (c) inhibited in presence of NO at 50% conversion and (d) promoted in presence of NO at temperatures above 450 °C.

At temperatures above 450 °C where surface coverages of the catalyst become negligible, NO converts to nitrates, which in turn boost the methane conversion.

Conclusion

By using complementary methods modulation-excitation XAS to study the structural dynamics of Pd and Pt sites, modelling the spectra theoretically, and at the same time investigating the overall surface adsorbates by infrared spectroscopy, we gained significant insight on the dynamics and the role of PdO and alumina surface for the mechanism of the dry methane oxidation and inhibition by water and NO. This approach is not only relevant for reactions of emission control but in general including those relevant during power-to-X processes.

The results obtained for monometallic Pd and bimetallic Pd—Pt catalysts show that ME-XANES is able to identify with high sensitivity extremely vague dynamic responses to the gas modulations. We found that these spectral responses were specific for exchange of stable surface species, which were assigned with the help of calculated XANES spectra on potential structures of Pd and Pt with adsorbed ligands.

The strength of the present study was owing to the fact that the reaction and inhibition does not cause bulk changes to the PdO structure, making conventional XAS without the sensitivity gained through MES useless. The catalyst was intentionally left in a highly oxidized state in order to avoid any bulk redox changes to the catalyst that may outweigh the vague spectral changes on interaction of PdO with adsorbates. This has a consequence in studying the role of the Pt dopant: ME-XANES has shown that Pt participates in the reaction and is important for e.g. oxidation of NO.

However, the normally accepted role of Pt to facilitate reducibility of the Pd—Pt system was not addressed here, and further work is necessary to clarify its role and structure in the bimetallic catalyst, after having undergone reductive pretreatment. Another strength of this study was that at all times the catalyst was in a working state set close to 50% conversion, and short-term inhibition by water and NO was easily observed and completely reversible, which is a pre-requisite of MES. The technically relevant topic of long-term deactivation was also observed here by a slightly decreasing conversion through the course of the experiments, and would be interesting to address further in the future.

Complementary to ME-XANES, surface adsorbates (formate, hydroxyl, nitrate/nitrite) that participate in the reactions could be assessed using DRIFTS accounting for the role of the alumina support in the storage of adsorbates transported from the PdO particles, as well as inhibition of the catalytic sites at the periphery of PdO and alumina.

With optimized model catalysts, using different supports, measurement conditions and more realistic theoretical models, the techniques presented here can give valuable new insight on the role of each of the components, leading to the design of better methane oxidation and in general heterogeneous catalysts.

Experimental Section

Catalyst synthesis

The catalysts were synthesized with a total noble metal loading of 2.4 wt.% by incipient wetness impregnation (IWI). For the bimetallic catalyst, a weight ratio of Pd:Pt = 5:1 was kept. Aqueous precursor solutions of tetraamminepalladium(II) nitrate (Chempur) and tetraammineplatinum(II) nitrate (Strem Chemicals) as well as their mixture for the bimetallic catalyst were prepared in the concentration for one cycle of IWI. 10 grams of γ-Al$_2$O$_3$ (Puraflox, BET surface area = 180 m^2/g, calcined at 700 °C for 5 hours, pore volume 0.85 cm^3/g determined with water) was impregnated with 8.5 mL of the respective precursor solution. The samples were dried overnight at room temperature, followed by 1 h at 70 °C to remove all moisture and calcined for 5 h at 500 °C in air. For calcination, the powder was homogenized and spread in a thin layer (1-2 mm) in large crucibles to ensure air access to all powder. A sieve fraction of 125–250 μm was prepared by pressing the powder into a pellet of area of 5 cm^2 at 10 tons, crushing and sieving.

ChemCatChem

Research Article
doi.org/10.1002/cctc.202200573

**Chemistry
Europe**
European Chemical
Societies Publishing

Characterization

The noble metal particle size and morphology was investigated on a Thermo Fisher Themis 300 transmission electron microscope (TEM) operated at 300 kV acceleration voltage in high-angle annular dark-field scanning mode. The particle size distribution was determined using ImageJ[38] by measuring > 400 particles in a series of images.

X-ray diffraction (XRD) patterns were acquired using a Bruker D8 Advance diffractometer using Cu Kα radiation ($\lambda = 1.54$ Å) generated by accelerating electrons over 40 kV at an anode current of 35 mA. The intensity of scattered X-rays was measured in a 2θ-range of 20–90°, step width of 0.0164°, 1 step/s.

The specific surface area was determined by N_2-physisorption at 77 K on a Rubotherm Belsorp-mini II instrument using the Brunauer-Emmet-Teller (BET) method with 3 points. Prior to the measurements, all samples were degassed at 300 °C for 2 h under vacuum.

The overall noble metal dispersion was determined using temperature-programmed desorption of CO (CO-TPD). The powder samples were placed in a tubular quartz glass reactor (ID = 8 mm). Prior to the measurements, the catalysts were pre-treated in air for 15 min at 400 °C, followed by a reduction in 4% H_2/N_2 at 400 °C for 30 min. Subsequently, the reactor was rapidly cooled down to room temperature under a N_2 flow. After saturating the catalyst with 1% CO/N_2 for 1 h, weakly adsorbed CO was removed by purging the reactor with pure N_2 for 45 minutes. TPD in a N_2 flow was performed by linearly ramping the temperature at 20 K/min up to 400 °C. All gas flows were kept at 500 mL/min. Gas concentrations of CO and CO_2 evolved during TPD were monitored by an NDIR detector (BINOS1000). For determining the noble metal dispersion (D), an adsorption stoichiometry of CO:(Pd,Pt) = 1:1 was assumed. Assuming a hemispherical geometry of the supported noble metal particles, average surface-based particle diameters (d_s) were calculated using the relation $d_s = 11.1/D$, using structural parameters of the noble metals listed in.[39] The dispersion D is a dimensionless factor between 0 and 1 and the diameter d_s is in nanometers.

X-ray absorption spectroscopy (XAS)

X-ray absorption spectroscopy measurements were performed at SOLEIL synchrotron (Saint-Aubin, France) at the ROCK beamline.[40] The storage ring was operated at 2.75 GeV with a ring current of 450 mA in top-up mode. ROCK is a bending-magnet beamline equipped with a horizontally focusing toroidal mirror inside the shield wall of the storage ring in order collect the maximum number of photons. A quick-scanning EXAFS (QEXAFS)[41] monochromator equipped with Si(111) and Si(220) channel-cut crystals were operated at 2 Hz for data acquisition at the Pt L_3-edge (11564 eV, flux at sample position 10^{12} ph/s) and the Pd K-edge (24350 eV, flux at sample position 10^{11} ph/s) respectively. Higher harmonics were removed by the collimating and vertically focusing mirrors upstream and downstream of the monochromator with Pd stripes for Pt L_3-edge measurements and Pt stripes for Pd K-edge measurements. The beam was focused to a size of 100 μm vertical by 200 μm horizontal at the sample position and vertical slits were used to block diffuse scattering. Incident and transmitted beam intensity was measured consecutively by 2 arrays of 3 ion chambers (OKEN) pre-filled with the optimal gas mixtures for the two edges, the arrays mounted above each other on a pneumatic stage for rapid switching. The sample was placed between the position of the 1st and 2nd ion chambers; Pt and Pd foils were placed between the 2nd and 3rd ion chambers in respective arrays for energy calibration. Automatized energy changes including monochromator crystal swap and mirror alignment took approximately 3 minutes.

In situ XAS setup

The catalytic experiment at the beamline was conducted using a quartz capillary reactor setup used for synchrotron-based *in situ* spectroscopy studies.[9] Ca. 30 mg of the Pd–Pt/Al_2O_3 and Pd/Al_2O_3 catalysts were loaded into 3 mm quartz capillaries (Hilgenberg). The catalyst bed of ca. 9 mm length was fixed between plugs of quartz wool. Heating was provided by a hot air gun (Gas Blower system, FMB-Oxford) as reported previously.[8] The temperature was controlled by a Eurotherm 2408 controller with a K-type thermocouple inside the Gas Blower.

Pure and mixed gases from gas cylinders (Air Liquide, purity > 4.5) were dosed by mass flow controllers (MFCs, Bronkhorst EL-FLOW). Gas mixtures in balance helium were composed of 4000 ppm CH_4, 10% O_2 and optionally 200 ppm NO and ca. 1% H_2O added via a saturator at room temperature. In the following, gas compositions will be referred to only by the components, present in concentrations stated above. A total gas flow of 50 mL/min was applied, corresponding to a space velocity of 50000 h^{-1}. Reaction products were analyzed by a quadrupole mass spectrometer (Thermostar, Pfeiffer Vacuum).

X-ray absorption near-edge structure (XANES) and extended fine-structure (EXAFS) data analysis

The raw data were processed using the Athena interface of the Demeter software package.[42] The spectra were merged and normalized. The oxygen-to-noble-metal ratio (O/Pd and O/Pt) was estimated by linear combination analysis of the X-ray absorption near-edge structure (XANES) spectra of the catalysts with those of PdO (Chempur), PtO_2 (Aldrich) and the respective metal foils.

The extended X-ray absorption fine structure (EXAFS) was extracted in k-space and Fourier-transformed on the range $k = 3.0$–12.5 $Å^{-1}$ for both Pd K and Pt L_3-edge spectra. Phase shifts and amplitudes for relevant back-scattering paths were calculated using FEFF6. EXAFS refinement was carried out in R-space using the Artemis interface of the Demeter software. An R-range of 1.0–3.7 Å was used. According to the Nyquist criterion, a maximum of 16 parameters could be extracted from the EXAFS data in this range. An electronic amplitude reduction factor of $S_0^2 = 0.78 \pm 0.04$ for the Pd K-edge and $S_0^2 = 0.77 \pm 0.04$ for Pt L_3-edge were determined from fitting the EXAFS spectra of corresponding metal foils.

Modulation-excitation XAS

Modulation was carried out by periodically switching between the standard reaction mixture at a temperature for 50% conversion and a modified atmosphere, where methane conversion was significantly lower. In this way, the chemical role of the noble metal during reaction and inhibition can be uncovered. Firstly, the effect of methane cut-off is investigated by variation between a methane-containing oxygen-rich gas flow and a methane-free one. Secondly, inhibition by water is studied by switching between a dry and wet reaction mixture and thirdly, inhibition by NO is studies in an analogous manner.

To detect structural changes, the time-resolved spectral series is demodulated by applying to it a Fourier filter with the frequency of the external modulation. The in-phase demodulated spectra can be viewed as difference spectra between the state of the catalyst in the first half of the modulation period and that in the second half.

ChemCatChem

Research Article
doi.org/10.1002/cctc.202200573

Chemistry Europe
European Chemical
Societies Publishing

For interpretation, demodulated spectra can be qualitatively and quantitatively compared to difference spectra between known reference compounds.

Modulation excitation XAS was conducted in order to amplify changes from static spectator species in the electronic structure of Pd and Pt while changing from high-conversion to low-conversion reaction conditions. The experiments were conducted isothermally at temperatures T_{50}, where approximately 50% methane conversion was achieved in the dry reaction mixture ($CH_4 + O_2$). Using a remotely-controlled four-way valve, periodic gas switches were conducted, so that dry mixture was dosed for 3 minutes, followed by a modified gas mixture for 3 minutes, a full period of 6 minutes. The modified gas mixtures were (i) O_2 in He, (ii) $CH_4 + O_2 + H_2O$ and (iii) $CH_4 + O_2 + NO$. In order to obtain significant statistics, a total of 10–15 periods were carried out while measuring either at the Pd K or the Pt L_3-edge once the repeatable and reversible catalytic performance decrease and increase has been established in response to the gas modulation.

MES data analysis was carried out using MATLAB. The QEXAFS spectra corresponding to an integral number of periods were first selected by correlating the time stamp of the QEXAFS data with the online gas analysis data. On the order of 10^4 spectra were normalized and averaged into one period of 36 spectra.[16a,43] The resulting time-resolved spectra $\mu(E, t)$ were demodulated by multiplying each point by a sine function of $T = 360$ s period, considering phase-shifts $\Delta\phi$, $0° \leq \Delta\phi < 360°$, and normalizing by the period duration [Eq. (1)]:

$$\mu(E, \Delta\varphi) = \frac{2}{T}\int_0^T \mu(E, t)\sin\left(\frac{360°}{T}t + \Delta\varphi\right)dt \quad (1)$$

The demodulated spectrum $\mu(E, \Delta\phi)$ with phase-shift zero ($\Delta\phi = 0°$) thus corresponded to a difference spectrum between the active catalyst under the dry reaction mixture and that under the modified reaction mixture.

XANES calculations

For comparison and qualitative analysis, molecular models of Pd and Pt on a PdO matrix were built using Avogadro[44] and geometrically optimized in a Universal force field. XANES spectra of the models, as well as bulk PdO, Pd, PtO_2 and Pt, were calculated until $k = 4.0$ Å^{-1} using FEFF 9.9.1[45] using Hedin-Lundquist exchange-correlation potentials, self-consistent field (SCF) radii of around 3.5 Å, corresponding to 2 coordination shells and full multiple-scattering (FMS) radii of around 9.5 Å were used. The COREHOLE FSR card (final-state rule) was used for the Pd K-edge and COREHOLE NONE for the Pt L_3-edge. The stoichiometry of the atoms was adjusted for a realistic determination of the Fermi level, in that the absorber and ligands were weighted by 1, neighboring Pd and O atoms by 100 to stabilize their constant contribution, and any ligands on neighboring atoms by 0.001, the lowest stoichiometry possible to make their contribution negligible.

In situ DRIFTS

DRIFTS data were recorded on a Bruker VERTEX 70 spectrometer equipped with diffuse-reflectance optics (Praying Mantis, Harrick) and an *in situ* cell (Harrick) for heating in a gas flow. The sample powder in a sieve fraction 125–250 μm was placed in the sample cup (6 mm diameter and 3 mm depth) and the cell was closed with a dome cover with KBr windows. The gas passed the sample from the top of the cup and exited through a wire mesh at the bottom.

Gases (Air Liquide, purity 5.0) were dosed using mass flow controllers and mixed before being directed to the cell. Water vapor was dosed via a saturator in a He flow at room temperature. The gas composition contained 4000 ppm methane, 10% oxygen and balance helium. The total flow was 200 mL per minute. 200 ppm NO and 1% H_2O were dosed with a four-way valve, as for the XAS experiments. The gas composition at the exit of the cell was analyzed by mass spectrometry.

DRIFTS spectra were acquired in reflectance mode ($R = I_r/I_0$) and converted to the Kubelka-Munk function $KM(R) = \frac{1}{2}(1-R)^2/R$, where I_r is the reflected intensity and I_0 the "incident intensity" measured in diffuse reflectance mode of monocrystalline CaF_2 (sieve fraction 125–250 μm). The measurements of CaF_2 were conducted at temperatures of the catalyst measurements to take the significant contribution of black-body radiation into account.

A 2.4% Pd/Al_2O_3 catalyst was baked out in the DRIFTS cell in a flow of O_2 in helium at 600°C and background spectra were acquired at 550°C and 350°C in this gas flow. The reported temperature is the setpoint, applicable to the circumference of the sample cup, whereas the temperature at the center of the catalyst which was probed by the infrared beam was approximately 150 K lower. The background spectra correspond to the surface chemistry of a clean catalyst surface. Subsequently at 550°C, the catalyst was exposed to the reaction mixture ($CH_4 + O_2$) for 15 minutes to reach steady-state conditions, and the first spectrum was taken to study the evolution of species appearing during reaction. The catalyst was then baked out and the experiment repeated at 350°C. After running under reaction conditions, water vapor or NO was added for a further 15 minutes, after which spectra were taken. These steps were repeated for both 350°C and 550°C, baking out the catalyst in between the experiments. To probe non-catalytic reaction mechanisms, the entire DRIFTS protocol mention above was conducted with pure Al_2O_3 from the same batch that was used for catalyst synthesis. Results are reported as difference spectra between the initial reaction mixture and the baked-out state, as well as difference spectra between the reaction mixture with water or NO and the one without.

Conflict of Interest

The authors declare no conflict of interest.

ChemCatChem

Research Article
doi.org/10.1002/cctc.202200573

Chemistry Europe
European Chemical
Societies Publishing

Data Availability Statement

The data that support the findings of this study are available from the corresponding author upon reasonable request.

[1] H. Blanco, W. Nijs, J. Ruf, A. Faaij, *Appl. Energy* **2018**, *232*, 323–340.
[2] R. Gholami, M. Alyani, K. Smith, *Catalysts* **2015**, *5*, 561.
[3] K. Persson, L. D. Pfefferle, W. Schwartz, A. Ersson, S. G. Järås, *Appl. Catal. B* **2007**, *74*, 242–250.
[4] a) P. Hurtado, S. Ordóñez, H. Sastre, F. V. Díez, *Appl. Catal. B* **2004**, *47*, 85–93; b) M. Öcal, R. Oukaci, G. Marcelin, B. W. L. Jang, J. J. Spivey, *Catal. Today* **2000**, *59*, 205–217.
[5] K. F. Kalz, R. Kraehnert, M. Dvoyashkin, R. Dittmeyer, R. Gläser, U. Krewer, K. Reuter, J.-D. Grunwaldt, *ChemCatChem* **2017**, *9*, 17–29.
[6] a) N. M. Kinnunen, J. T. Hirvi, K. Kallinen, T. Maunula, M. Keenan, M. Suvanto, *Appl. Catal. B* **2017**, *207*, 114–119; b) B. Torkashvand, A. Gremminger, S. Valchera, M. Casapu, J.-D. Grunwaldt, O. Deutschmann, *SAE International* **2017**, 2017-2001–1019.
[7] a) D. Ciuparu, E. Perkins, L. Pfefferle, *Appl. Catal. A* **2004**, *263*, 145–153; b) W. R. Schwartz, D. Ciuparu, L. D. Pfefferle, *J. Phys. Chem. C* **2012**, *116*, 8587–8593.
[8] A. T. Gremminger, H. W. Pereira de Carvalho, R. Popescu, J.-D. Grunwaldt, O. Deutschmann, *Catal. Today* **2015**, *258*, 470–480.
[9] J.-D. Grunwaldt, N. v. Vegten, A. Baiker, *Chem. Commun.* **2007**, 4635–4637.
[10] a) Q. Zheng, R. Farrauto, M. Deeba, *Catalysts* **2015**, *5*, 1797; b) J.-D. Grunwaldt, N. van Vegten, A. Baiker, W. van Beek, *J. Phys. Conf. Ser.* **2009**, *190*, 012160.
[11] P. W. Albers, K. Möbus, S. D. Wieland, S. F. Parker, *Phys. Chem. Chem. Phys.* **2015**, *17*, 5274–5278.
[12] J. Bruns, T. Klüner, M. S. Wickleder, *Chem. Eur. J.* **2015**, *21*, 1294–1301.
[13] J. Lallo, S. A. Tenney, A. Kramer, P. Sutter, M. Batzill, *J. Chem. Phys.* **2014**, *141*, 154702.
[14] a) C. F. J. König, J. A. van Bokhoven, T. J. Schildhauer, M. Nachtegaal, *J. Phys. Chem. C* **2012**, *116*, 19857–19866; b) J. Nilsson, P.-A. Carlsson, N. M. Martin, E. C. Adams, G. Agostini, H. Grönbeck, M. Skoglundh, *J. Catal.* **2017**, *356*, 237–245.
[15] Y. Lu, S. Keav, V. Marchionni, G. L. Chiarello, A. Pappacena, M. Di Michiel, M. A. Newton, A. Weidenkaff, D. Ferri, *Catal. Sci. Technol.* **2014**, *4*, 2919–2931.
[16] a) A. Gaur, T. M. Hartmann Dabros, M. Høj, A. Boubnov, T. Prüssmann, J. Jelic, F. Studt, A. D. Jensen, J.-D. Grunwaldt, *ACS Catal.* **2019**, *9*, 2568–2579; b) A. Gaur, M. Stehle, M.-A. Serrer, M. Z. Stummann, C. La Fontaine, V. Briois, J.-D. Grunwaldt, M. Høj, *ACS Catal.* **2022**, *12*, 633–647.
[17] S. Czioska, A. Boubnov, D. Escalera-López, J. Geppert, A. Zagalskaya, P. Röse, E. Saraçi, V. Alexandrov, U. Krewer, S. Cherevko, J.-D. Grunwaldt, *ACS Catal.* **2021**, *11*, 10043–10057.
[18] M.-A. Serrer, A. Gaur, J. Jelic, S. Weber, C. Fritsch, A. H. Clark, E. Saraçi, F. Studt, J.-D. Grunwaldt, *Catal. Sci. Technol.* **2020**, *10*, 7542–7554.
[19] A. Urakawa, T. Bürgi, A. Baiker, *Chem. Eng. Sci.* **2008**, *63*, 4902–4909.
[20] P. Lott, P. Dolcet, M. Casapu, J.-D. Grunwaldt, O. Deutschmann, *Ind. Eng. Chem. Res.* **2019**, *58*, 12561–12570.
[21] V. R. Fernandes, M. V. d. Bossche, J. Knudsen, M. H. Farstad, J. Gustafson, H. J. Venvik, H. Grönbeck, A. Borg, *ACS Catal.* **2016**, *6*, 4154–4161.
[22] a) N. M. Kinnunen, J. T. Hirvi, M. Suvanto, T. A. Pakkanen, *J. Mol. Catal. A* **2012**, *356*, 20–28; b) P. Castellazzi, G. Groppi, P. Forzatti, *Appl. Catal. B* **2010**, *95*, 303–311; c) K. Persson, K. Jansson, S. G. Järås, *J. Catal.* **2007**, *245*, 401–414.
[23] W. Xu, G. Zhang, H. Shou, J. Zhou, S. Chen, S. Chu, J. Zhang, L. Song, *J. Synchrotron Radiat.* **2022**, *29*, 1065–1073.
[24] X. Li, X. Wang, K. Roy, J. A. van Bokhoven, L. Artiglia, *ACS Catal.* **2020**, *10*, 5783–5792.
[25] Z. Liang, L. Song, A. O. Elnabawy, N. Marinkovic, M. Mavrikakis, R. R. Adzic, *Top. Catal.* **2020**, *63*, 742–749.
[26] a) M. V. d. Bossche, H. Grönbeck, *J. Am. Chem. Soc.* **2015**, *137*, 12035–12044; b) H. Stotz, L. Maier, A. Boubnov, A. T. Gremminger, J. D. Grunwaldt, O. Deutschmann, *J. Catal.* **2019**, *370*, 152–175.
[27] T. R. Johns, J. R. Gaudet, E. J. Peterson, J. T. Miller, E. A. Stach, C. H. Kim, M. P. Balogh, A. K. Datye, *ChemCatChem* **2013**, *5*, 2636–2645.
[28] C. Keresszegi, T. Mallat, J.-D. Grunwaldt, A. Baiker, *J. Catal.* **2004**, *225*, 138–146.
[29] B. M. Weiss, E. Iglesia, *J. Catal.* **2010**, *272*, 74–81.
[30] X. Auvray, L. Olsson, *Appl. Catal. B* **2015**, *168–169*, 342–352.
[31] G. W. Smith, E. A. Carter, *J. Phys. Chem.* **1991**, *95*, 2327–2339.
[32] C. Li, G. Li, Q. Xin, *J. Phys. Chem.* **1994**, *98*, 1933–1938.
[33] C.-R. Florén, M. Van den Bossche, D. Creaser, H. Grönbeck, P.-A. Carlsson, H. Korpi, M. Skoglundh, *Catal. Sci. Technol.* **2018**, *8*, 508–520.
[34] P. Velin, F. Hemmingsson, A. Schaefer, M. Skoglundh, K. A. Lomachenko, A. Raj, D. Thompsett, G. Smedler, P.-A. Carlsson, *ChemCatChem* **2021**, *13*, 3765–3771.
[35] B. L. Mojet, S. D. Ebbesen, L. Lefferts, *Chem. Soc. Rev.* **2010**, *39*, 4643–4655.
[36] a) G. Busca, V. Lorenzelli, *J. Catal.* **1981**, *72*, 303–313; b) J. Sá, J. A. Anderson, *Appl. Catal. B* **2008**, *77*, 409–417.
[37] K. Hadjiivanov, E. Ivanova, M. Daturi, J. Saussey, J. C. Lavalley, *Chem. Phys. Lett.* **2003**, *370*, 712–718.
[38] ImageJ from National Institutes of Health, http://rsbweb.nih.gov/ij/, last accessed 14.04.2022.
[39] L. Spenadel, M. Boudart, *J. Phys. Chem.* **1960**, *64*, 204–207.
[40] V. Briois, C. La Fontaine, S. Belin, L. Barthe, T. Moreno, V. Pinty, A. Carcy, R. Girardot, E. Fonda, *J. Phys. Conf. Ser.* **2016**, *712*, 012149.
[41] R. Frahm, M. Richwin, D. Lützenkirchen-Hecht, *Phys. Scr.* **2005**, 974.
[42] B. Ravel, M. Newville, *J. Synchrotron Radiat.* **2005**, *12*, 537–541.
[43] J. Stötzel, D. Lützenkirchen-Hecht, R. Frahm, J. D. Grunwaldt, *J. Phys. Conf. Ser.* **2013**, *430*, 012126.
[44] M. D. Hanwell, D. E. Curtis, D. C. Lonie, T. Vandermeersch, E. Zurek, G. R. Hutchison, *J. Cheminf.* **2012**, *4*, 17.
[45] J. J. Rehr, J. J. Kas, F. D. Vila, M. P. Prange, K. Jorissen, *Phys. Chem. Chem. Phys.* **2010**, *12*, 5503–5513.